Renewable and Sustainable Energy Reviews 178 (2023) 113254

Contents lists available at ScienceDirect

Renewable and Sustainable Energy Reviews

journal homepage: www.elsevier.com/locate/rser

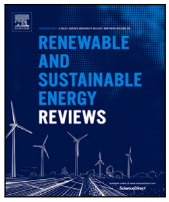

Original research article

Probabilistic analysis of wind turbine performance degradation due to blade erosion accounting for uncertainty of damage geometry

M. Sergio Campobasso [a,*], Alessio Castorrini [b,a], Andrea Ortolani [a], Edmondo Minisci [c]

[a] University of Lancaster, School of Engineering, Lancaster LA1 4YW, United Kingdom
[b] Sapienza University of Rome, Department of Mechanical and Aerospace Engineering, Via Eudossiana 18, 00184 Rome, Italy
[c] University of Strathclyde, Department of Mechanical and Aerospace Engineering, Glasgow G1 1XQ, United Kingdom

ARTICLE INFO

Keywords:
Wind turbine predictive maintenance
Leading edge erosion
Eroded blade aerodynamics
Uncertain field records of blade erosion
Probability distribution function of turbine energy yield
Stochastic and deterministic methods for uncertainty propagation

ABSTRACT

Geometry alterations of wind turbine blades due to erosion reduce the blade aerodynamic performance, yielding turbine power and energy losses. This study proposes a novel probabilistic analysis framework combining computational fluid dynamics, probabilistic and deterministic uncertainty propagation, and high-performance computing to assess this performance degradation accounting for the unavoidable uncertainty on field records of blade erosion. This uncertainty presently prevents using erosion records for improving wind turbine maintenance planning, increasing energy yield, and thus further reducing the wind energy cost. The technology is demonstrated by quantifying the statistical moments of power and energy yield losses of an eroded utility-scale turbine at a North Sea offshore site and a southern European onshore site. The expectations of the offshore and onshore annual energy production losses are found to be 2 and 3% of the corresponding nominal values, respectively, with corresponding standard deviations of 0.1 and 0.15%. In the realistic scenario of erosion varying with high radial frequency, these low standard deviations result from partial compensation of the impact of mild and severe damages. These low standard deviations indicate that present uncertainty levels of erosion geometry records can be handled with uncertainty analysis in predictive maintenance for further reducing wind energy costs. With the frequent assumption of small or no radial variation of erosion, the standard deviation of the loss is misleadingly higher. For the first time, the study reports on the significant impact of turbulence intensity of the installation site on the turbine loss variability with the site wind characteristics.

1. Introduction

The geometry alterations of the leading edge (LE) of rotating machine blades caused by harsh operating conditions [1] is receiving growing attention, because of the detrimental impact the resulting aero- or hydrodynamic performance degradation has on operation and maintenance (O&M) costs, cost of energy (in the case of renewable energy generation), and fuel consumption and carbon emissions (in the case of aeronautical propulsion). Adopting the terminology of [1], blade surface perturbations can be caused by additive or subtractive processes. Examples of additive processes include ice accretion [2,3], dust accumulation [4] and insect accumulation [5] on wind turbine blades, and biofouling of the blades of tidal current turbines [6–8].

LE erosion (LEE) of wind turbine blades [9] is a notable case of subtractive process, and is often due to the high-speed impact of the blade LE with rain droplets or hail stones [10]. The peripheral speed of the outboard part of wind turbines, particularly in offshore wind farms, is approaching 90 to 100 m/s, with higher tip speeds being appealing for several reasons, including higher aerodynamic efficiency, and lower cost of gearboxes and drivetrains [11].

Wind turbine blade LEE, the key focus of this study, is an unresolved problem of the wind energy industry. LEE increases the drag and reduces the lift acting on the turbine blades, thus reducing the torque at the rotor hub. The resulting reduced power decreases the turbine Annual Energy Production (AEP) [12], and increases O&M costs for blade repair [13]. In early 2016, the revenue loss of the European offshore wind energy industry caused by the AEP lost to LEE was estimated between €56 million and €75 million a year [9]. The present value of the revenue loss of the offshore and onshore wind energy industry in Europe is expected to be about one order of magnitude larger, because the onshore wind capacity is at least five times the offshore capacity, and LEE losses are larger in onshore wind farms. Furthermore, this loss is expected to grow, since the overall installed wind capacity is constantly and rapidly growing to meet carbon emission requirements. The increase of the levelized cost of energy due to these AEP losses

* Corresponding author.
E-mail address: m.s.campobasso@lancaster.ac.uk (M. Sergio Campobasso).

https://doi.org/10.1016/j.rser.2023.113254
Received 28 November 2022; Received in revised form 15 February 2023; Accepted 7 March 2023
Available online 14 March 2023

is further aggravated by the costs of unplanned maintenance incurred to repair the eroded blades. Notable examples are the LEE-prompted interventions at the 630 MW London Array [14] and the 400 MW Anholt wind farm [15] in 2018.

One of the targets of blade design is to maintain blade boundary layers (BLs) laminar for as long as possible after they originate at the LE stagnation point. This yields improved lift and drag characteristics with respect to fully turbulent BLs from the LE. Even when blade surfaces are smooth, however, laminar-to-turbulent transition [16] occurs before the trailing edge (TE), due to the adverse pressure gradient on the rear part of the blade sections. The existence of LE geometry perturbations, such as increased surface roughness, results in premature BL transition. Above a critical value of LE roughness, the so-called critical roughness height [17], blade BLs are fully turbulent from their onset.

The aerodynamic performance loss of the turbine blades, and the resulting power reduction can be well above the level corresponding to the loss of BL laminarity caused by low-level LE roughness at the onset of the erosion process. LEE can progress to levels at which accurately estimating power losses requires resolving the erosion geometry, an information often affected by uncertainty. In general, the phenomena responsible for the blade performance reduction, and the magnitude of this reduction depend on the pattern and extent of the LE surface damage, which, in turn, depends on the stage at which LEE is. The onset and progression of LEE are site-dependent [12,18,19]. Initially, erosion alters the surface geometry at microscale levels, leading to increased roughness. When the material reaches the damage incubation limit [20], small pits appear on the surface. At a more advanced stage, the pit size increases, and groups of pits coalesce in larger gouges. As erosion progresses, larger amounts of material are lost, also along the adhesion boundaries between different material layers, and LE grooves are formed. The four subplots of Fig. 1 [21] provide an example of the aforementioned LEE stages using photographs of real blade LEs. Photographs (A) to (D) illustrate the progression from increased surface roughness to a LE featuring chordwise grooves of varying length and depth along the blade length.

Any LE material loss caused by erosion leads to increased roughness. When the erosion level is low, comparable with the critical roughness height, performance losses are caused by the loss of BL laminarity, and also an additional viscous stress increase due to roughness. The performance reductions due to these levels of LEE have been extensively studied, for example by using grit roughness and grit tape in wind tunnel testing [22], and distributed roughness models in Computational Fluid Dynamics (CFD) simulations [23]. When the erosion level grows above the critical roughness height, the dependence of the aerodynamic performance loss on the erosion geometry becomes stronger [24], and the performance loss becomes higher than that caused by the loss of BL laminarity [25,26]. At this stage, it becomes essential to *resolve* the erosion geometry, in both wind tunnel testing and CFD simulations [27], to avoid underestimating the performance reduction of the blade sections.

The discussion above points to the importance of acquiring in as much detail as possible the geometry of LEE, when one intends to use this information to assess the power and AEP losses of individual wind turbines or entire wind farms. An accurate method for blade surface condition monitoring consists of taking off the blades and using 3D laser scans to measure position and size of the blade perturbations. This operation is costly and time-consuming, and thus not used routinely. The most widespread optical inspection technique presently relies on high-resolution camera footage acquired by ground-based operators or, increasingly, drone-mounted high-resolution cameras and/or lidars [28–30]. Thus, routinely acquired LEE geometry records are affected by uncertainty, in that they do not have the completeness and/or resolution needed for a reliable power and AEP loss assessment. This uncertainty is a key factor preventing the assessment of the power performance degradation of operational turbines caused by LEE.

The issue of the uncertainty in the predictions of turbine loads and AEP resulting from both stochastic deviations of the blade surface from its nominal geometry, and the variability of the site mean wind speed, was first discussed in [31]. Stochastic perturbations such as LE and TE alterations due to manufacturing/assembly errors, LE erosion, insect and dust accumulation were modeled as stochastic variations of the lift and drag curves and the radial extent of these perturbations. In a later study, CFD was used to determine the lift and drag curves of the damaged airfoils [32]. Both studies viewed the uncertainty problem from a design perspective, thus taking the nominal turbine as the upper end of the variability ranges of all uncertain input variables.

The main objectives of this study are to present a comprehensive probabilistic framework enabling the use of uncertain LEE records in turbine performance assessment, and demonstrate its use by thoroughly investigating key aspects of wind turbine performance degradation due to LEE never addressed before. These include (*a*) the quantification of both expectation and standard deviation of turbine power and AEP losses due to uncertain but realistic LEE field records for representative offshore and onshore wind farm sites, (*b*) the assessment of the relative weight of site turbulence intensity (TI) and mean wind speed on power and AEP losses, and (*c*) the investigation of the probabilistic sensitivity of performance and energy loss to the resolution of the LE damage along the blade length. The study also demonstrates the reliability and high computational efficiency of a deterministic uncertainty propagation technology, the Univariate Reduced Quadrature (URQ) method [33], for the probabilistic assessment of wind turbine performance degradation due to uncertain LEE geometry. The findings of this study are expected to prompt new research in most areas of LE erosion, and, on the industrial side, benefit wind turbine designers, wind farm operators, and wind farm O&M. In this sector, this research paves the way to *predictive maintenance*, whereby one balances trade-offs of projected AEP revenue loss and costs of blade repairs in blade maintenance planning.

Section 2 formulates the probabilistic problems addressed in this study, defining the reference turbine and the characteristics of the reference offshore and onshore sites. The selected LEE geometry representation is also reported. Section 3 describes the methodology of the investigation, focusing on (*a*) the Monte Carlo (MC) uncertainty propagation (UP) method used to wrap the deterministic AEP Loss Prediction System (ALPS) analysis [26,34], (*b*) the wind turbine analysis code used by ALPS, and (*c*) the computational aerodynamics method used to generate all airfoil force coefficients. To provide key background for the discussion on the turbine performance analyses, Section 4 investigates the global sensitivity of damaged airfoils to the parameters of the geometry perturbations. The main results are provided in Section 5, made up of five parts. Reducing the problem complexity by adopting a groove model of severe LEE damage, Section 5.1 investigates the deterministic sensitivity of the damaged turbine performance to the damage geometry, an analysis required before investigating the probabilistic sensitivity with the subsequent more realistic problem formulations. Section 5.2 turns to realistic geometry complexities, and studies the probabilistic performance degradation of offshore turbines accounting for uncertainty on one or all of the LEE damage parameters. In Section 5.3 the probabilistic ALPS framework is used to assess the sensitivity of mean and standard deviation of the turbine AEP to the resolution of the damage geometry along the affected blade length. In Section 5.4, the application of the URQ UP method to the problem at hand is illustrated, demonstrating a substantial computational cost reduction over the MC approach. The probabilistic analysis of the LEE-induced turbine performance drop at the onshore site is presented in Section 5.5, which also investigates the relative weight of TI and mean wind speed in the variation of AEP losses between offshore and onshore sites. The key findings of the study are summarized in Section 6.

2. Problem definition

One of the aims of this study is to assess the impact of the uncertainty on blade LEE geometry on the variability of turbine power and

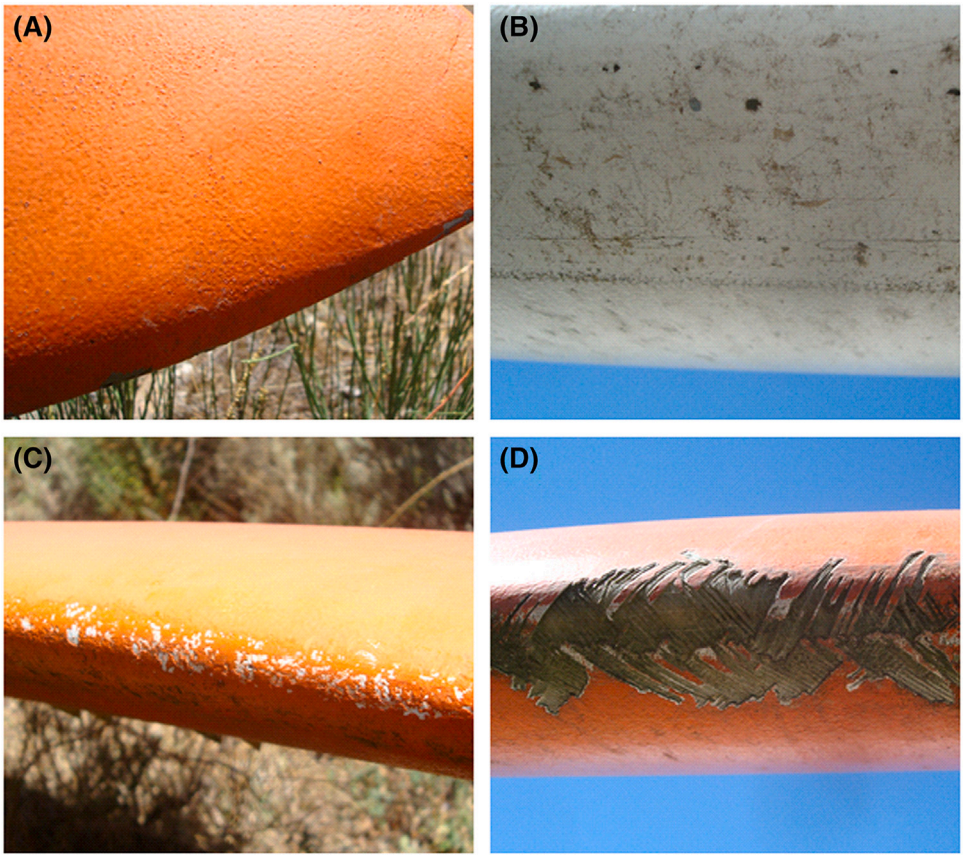

Fig. 1. Example of LEE progression [21]. (A): increased surface roughness; (B): formation of pits; (C): coalescence of pits into larger gouges; (D): LE delamination.

AEP loss. In the probabilistic framework described below, the problem corresponds to determining the AEP Probability Distribution Function (PDF) or, at least, its first two statistical moments, for given uncertainty intervals of LEE geometry perturbations. The baseline turbine of this study is the NREL 5 MW reference turbine [35]. In all analyses, the power and AEP losses of turbines with uncertain LEE geometry are relative to the power and AEP of the baseline NREL 5 MW turbine, which features nominal blade geometry with free laminar-to-turbulent transition of the blade BLs. The rotor has a radius of about 63 m, and the damaged blades are supposed to be affected by LEE only from 70% of the rotor radius to the blade tip. The largest extent of LEE is typically observed at the highest rotor radii, because the LE damage increases with the relative impact speed of LE and airborne particles, and the blade local peripheral speed, which grows with the radius, is the largest component of the relative impact speed. Field observations [36] and numerical studies [37] indicate that LEE is rather weak below 70% rotor radius, which is the reason for the choice made in this study. It is also noted that the analyses of this study do not account, either deterministically or probabilistically, for the expected reduction of the LEE severity as the blade section radius decreases. This feature will be added in future extensions of this work.

The nominal blades use the NACA 64_3-618 airfoil from 70% of the rotor radius to the blade tip. The LEE geometry model consists of the three-parameter LE groove depicted in Fig. 2. The groove is parametrized by its depth d, its curvilinear extension s_u on the upper side measured from the LE, and its curvilinear extension s_l on the lower side, also measured from the LE. For positive values of the Angle of Attack (AoA) α, the upper side corresponds to the suction side (SS), and the lower side to the pressure side (PS).

The uncertainty on the groove geometry is accounted for by taking one or all three groove parameters to be uniformly distributed random variables. The mean, minimum and maximum values of the three uniform distributions, normalized by the chord c, are provided in Table 1.

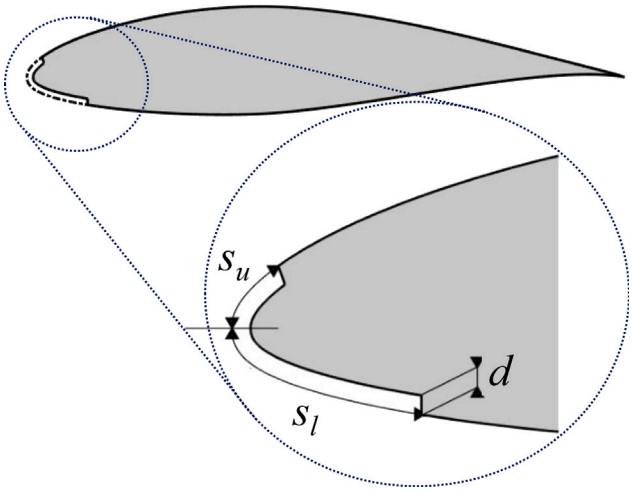

Fig. 2. Geometry parametrization of LE groove of NACA 64_3-618 airfoil.

The groove-based parametrization of LEE is a representation frequently adopted in previous studies [32,34,38]. The mean values of the three parameters correspond to medium to severe erosion damage, according to LEE geometry data available in [39], which, in turn, are based on the analysis of the erosion geometry of utility-scale turbine blades in service or maintenance. The uncertainty ranges of the three parameters are deliberately broad to reflect the uncertainty associated

Table 1
Variability range of three geometry parameters defining LE erosion grooves of NACA 64_3-618 airfoil.

	Mean	Min.	Max.
$d/c \cdot 100$	0.4	0.1	0.7
$s_u/c \cdot 100$	1.9	1.0	2.8
$s_l/c \cdot 100$	2.47	1.3	3.64

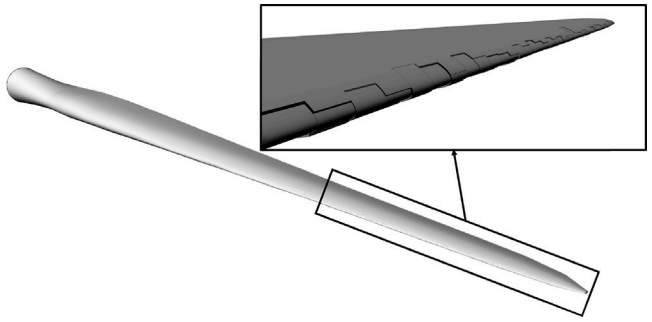

Fig. 3. Complete view of the blade of the NREL 5 MW turbine (left), and enlarged view of its grooved outer portion.

with the fairly qualitative nature of the erosion geometry data collected with common blade inspection methods.

Unless otherwise stated, the outer 30% of the blade is subdivided in 50 strips of equal radial length of 0.38 m. Each strip features a grooved NACA 64_3-618 airfoil, and each uncertain groove parameter is sampled from the associated uniform distribution. A view of the whole blade is provided in the left part of Fig. 3, and an enlarged view of the grooved blade portion is shown on the right.

The analyses of Section 5 consider several scenarios, including the case in which all three LE groove parameters are uncertain, and the case in which only the groove depth is uncertain. Moreover, in order to analyze the dependence of mean and standard deviation of power and AEP losses on the radial resolution of the LEE geometry, the three groove geometry parameters will be assumed to vary randomly and independently in all 50 blade strips, in 10 sets of 5 adjacent strips, and 5 sets of 10 adjacent strips.

The probabilistic problem under investigation is formulated for both a reference offshore and a reference onshore site. This is done because the percentage AEP loss due to erosion depends on the scale factor and the shape factor of the site-specific Weibull wind frequency distribution [26], with the former parameter depending linearly on the mean wind speed for set value of the latter, and the shape factor providing a measure of the wind speed spread about the modal value of the distribution. The percentage AEP loss depends also on the site TI, and this dependence, previously overlooked, is analyzed below. The reference offshore site is representative of typical offshore wind farm locations in the North Sea. The selected mean wind speed at the turbine hub height of 90 m is 9.36 m/s, and the scale factor is 2, with the choice of these two values yielding a scale factor of 10.56 m/s. The choice of the scale and shape factors affects the turbine AEP because it determines the available wind resource. The freestream TI also affects the turbine AEP through variations of the turbine mean power curve [40]. For the offshore site, the TI values adopted for each wind speed are those measured in the FINO1 experiment in the North Sea [41,42], with the mean value of this parameter being around 5%. The calculation of the turbine power curves reported below also requires the vertical profile of the mean wind speed. The vertical mean wind speed ahead of the turbine has been determined with the power law, setting the shear exponent γ to 1/7.

The reference onshore site is representative of one of the windiest onshore sites in Italy, located in the southern region of Puglia (41° 18′ 56″ N, 15° 8′ 44″ E). The turbine hub height at the onshore site is taken to be 100 m, 10 m higher than the offshore turbine, to partly compensate for the lower energy yield of onshore sites due to lower mean wind speeds. The mean wind speed at the hub height is 7.84 m/s, and the shape factor is 1.88 [43], with the choice of these two values yielding a scale factor of 8.8320 m/s. Also for the onshore site, the vertical mean wind speed is determined with the power law, setting the wind shear exponent to 0.2. The onshore site TI for each wind speed is set using the guidelines of the International Standard IEC61400 of the International Electrotechnical Commission for a site of class B. Using these guidelines [44], TI for each wind speed is given by:

$$TI = TI_{ref}(0.75 + 5.6/\overline{V}) \tag{1}$$

where TI_{ref} has been set to 14% and $\overline{V}$ is the mean wind speed.

3. Methodology

The ALPS analysis framework, which is central to the present study, was first presented in [34], and its capability of determining deterministic turbine power and AEP losses due to LEE damage by sparse pits and gouges, and LE grooves was demonstrated in [26]. ALPS has a modular structure, and it presently uses the wind turbine engineering code OpenFAST [45] to determine the power curve and the loads of turbines with general blade geometry. OpenFAST handles rotor aerodynamics by means of the blade element moment theory (BEMT) code AeroDyn [46], which, for each blade strip or section, requires the curve $c_l(\alpha)$ of the lift coefficient for all AoAs of interest, and the curve $c_d(\alpha)$ of the drag coefficient. These two curves depend on the geometry of the blade section, and can be computed with CFD. When dealing with a large set of damaged blade sections, the calculation of these two curves can be accelerated by pre-computing them for large sets of baseline damages, and using machine learning to rapidly determine these curves for damaged sections not included in the databases [26]. In the present study, however, all $c_l(\alpha)$ and $c_d(\alpha)$ curves have been calculated directly with CFD, as explained below. Once the power curve of a damaged turbine is computed, and a site is selected, the AEP is computed by integrating the wind frequency distribution against the power curve, and the AEP loss is given by the difference of the AEP of the nominal turbine and that of the damaged turbine.

When defining the LEE geometry perturbations with PDFs, the calculation of the turbine power curve and the site-dependent AEP require using UP to obtain a probabilistic estimate of these outputs. The UP process always requires multiple ALPS analyses to propagate uncertainty through the turbine analysis chain. In this study, all randomly perturbed blade geometries are defined first. Then, ALPS is wrapped by a loop that runs it for all these perturbed turbines to propagate the LEE geometry uncertainty. Depending on the adopted UP method, this loop yields the first few statistical moments of power and AEP PDFs, or even the complete PDFs, when using MC sampling.

The set-up of the MC analyses used for UP is discussed in Section 3.1. The set-up of the OpenFAST calculation of the power curve of each damaged turbine is described in Section 3.2. The computational aerodynamics method used to determine the database of the force coefficients of the damaged airfoils in the analysis domain defined by Table 1 is reported in Section 3.3.

3.1. Uncertainty propagation

The main UP method adopted to propagate the LEE geometry uncertainty is MC sampling. The three ranges of the erosion geometry variables in Table 1 are subdivided in six intervals, yielding seven possible values in each range. Thus, the considered discrete analysis space consists of $7^3 = 343$ damaged variants of the NACA 64_3-618 airfoil, whose $c_l(\alpha)$ and $c_d(\alpha)$ curves are calculated using the computational aerodynamics set-up defined in Section 3.3. The choice of seven points to discretize the range of each erosion geometry variable resulted

from an optimal trade-off of computational cost and smoothness of the contour maps of the percentage variation of the aerodynamic force coefficients plotted against the groove geometry parameters. A trade-off arises because the computational cost decreases as the number of required aerodynamic analyses is reduced, and the contour map smoothness increases with the number of points (i.e. damaged airfoil variants) used to discretize the damage intervals. Since the damaged blades have up to 50 distinct grooved NACA 64_3-618 sections from 70% rotor radius to blade tip, the erosion geometry of each rotor is defined by up to 150 LEE geometry variables. As the three ranges of the groove geometry variables are discretized with seven points, the largest number of possible eroded rotors is 7^{150}. When the uncertainty on all three groove variables is propagated through the turbine analysis system, the resulting distributions of power and AEP can be viewed as *joint* PDFs.

Integer MC sampling is used in all analyses herein. Therefore, when all three groove parameters are uncertain, only the triplets of parameters that belong to the Cartesian product of the three seven-point ranges are admissible groove geometries. The discrete MC sampling is accomplished by using the MATLAB random real number generator `rand`, which samples the interval [0,1] assuming a uniform distribution. In the implemented sampling, the conversion from real to integer relies on the MATLAB function `round`, embedded in the MATLAB equation:

$$\texttt{round(rand()} * (N + \Delta/2 - (1 - \Delta/2)) + \Delta/2) \tag{2}$$

where N is the number of damaged variants of the NACA 64_3-618 airfoil, $\Delta = 1$, and the MATLAB function `round` rounds its real argument to the nearest integer value.

The probabilistic power and AEP investigations of Section 5 also consider scenarios in which only one of the three groove parameters is uncertain, with the other two set to constant values. This corresponds to determining *marginal* power and AEP PDFs, rather than joint PDFs of the case in which all independent variables are taken to be uncertain. When only one variable of the groove geometry of all 50 blade strips varies randomly and independently, the discrete analysis space of the marginal power and AEP PDFs has 7^{50} possible blade geometries, since each of the 50 eroded blade strips is defined by a single variable that can take seven discrete values.

3.2. Wind turbine performance analysis

The power curve of the nominal turbine and all its damaged variants are computed with OpenFAST version 3.0.0 - dev (Jan. 2022), assuming the turbine structure and its foundations to be rigid. In the BEMT model, both the grooved and the nominal blades are discretized with 50 strips from blade tip to 70% rotor radius, and 12 strips from 70% rotor radius to blade root. For both the offshore and onshore sites, the power curves are computed using turbulent inflow conditions, with the TI and wind shear data in Section 2. For each wind speed and TI, the space- and time-dependent turbulent wind is generated with the TurbSim code [47]. Each power curve is determined running OpenFAST for 21 wind speeds between cut-in and cut-out, and each analysis runs for 630 physical seconds with time-step of 0.01 s. Mean values of all output quantities, including rotor power and loads, are computed by averaging their time–history over the last 600 s of the simulation. The OpenFAST rotor speed and blade pitch control [35] is used in all simulations.

3.3. Computational aerodynamics and force coefficient database

The $c_l(\alpha)$ and $c_d(\alpha)$ curves of the nominal and grooved NACA 64_3-618 airfoils are computed by simulating their turbulent viscous flow field with the Navier–Stokes CFD code ANSYS FLUENT [48] version 2019 - release 3. The flow field past each airfoil is modeled as a 2D incompressible air flow. The pressure-based Reynolds-averaged Navier–Stokes (RANS) equations are coupled with Menter's two-equation $k-\omega$ shear stress transport (SST) model [49]. The space discretization of the convective fluxes of all transport equations, including those of the laminar-to-turbulent transition model summarized below, uses a second order upwind scheme, whereas all diffusive fluxes are discretized using second order finite-differencing. The numerical integration uses the COUPLED solver, whereby the continuity and momentum equations are solved in a strongly coupled fashion, and all other transport equations are solved in a loosely coupled fashion.

Modeling of the laminar-to-turbulent transition of the blade airfoil BLs is accomplished by solving two additional transport equations coupled to the SST turbulence model. The resulting model is the four-equation $\gamma - Re_\theta$ SST model [50–52]. The default value of the constant a_1 in the equation of the eddy viscosity μ_T [49] is 0.31. However, it was found in [53] and studies cited therein that a lower value, between 0.28 and 0.29, often enables improving the agreement of computed and measured $c_l(\alpha)$ curves of wind turbine airfoils. For this reason, $a_1 = 0.29$ has been used in all CFD simulations herein.

All meshes have a structured C-grid topology, consist of 115,449 quadrilateral cells, and have 456 cells along the airfoil surface and 150 cells in the normal direction. The curvilinear length of all grooves is covered by 100 cells. The airfoil chord c is set to 1 m in the numerical model, and the far field boundary is at $50c$ from the airfoil in all directions. The minimum distance of the first cell centers off the airfoil surface from this boundary is 1.3×10^{-6} m, and, for the chord-based Reynolds number of 9M adopted in all simulations, the maximum nondimensionalized wall distance y^+ has always been found to be less than 1.5. Views of the grid past the nominal airfoil and its LE are provided in Fig. 4(a), whereas views of the grid past the grooved airfoil and its LE, for the case of the mean groove defined by the mean values of d/c, s_u/c and s_l/c in Table 1, are reported in Fig. 4(b).

All CFD analyses of this study are time-dependent, because numerical instabilities were encountered in some of the analyses when using the steady state solver, particularly at the highest AoA values, characterized by TE flow separation and vortex shedding. The flow simulation for each AoA uses 3000 time-steps, with a time-step of 2.5×10^{-3} s, and 25 sub-iterations at each physical time. This parameter choice results in good convergence levels of all simulations, with an average residual drop of about three orders of magnitude. The choice of the time-step of 2.5×10^{-3} s is based on the assumption that the nondimensionalized frequency of the TE vortex shedding at high AoA, expressed by the Strouhal number, has an order of magnitude comparable to that of a circular cylinder. Based on experimental measurements of the vortex shedding behind a cylinder at high Reynolds number [54], a Strouhal number of about 0.25 has been assumed for the considered airfoil flow unsteadiness. The choice of 128 time interval per period has led to the indicated time-step. The far field TI of all CFD simulations is set to 0.1%, and the turbulent length scale at the far field boundary is set to $0.2c$, as this value minimizes the reduction of TI between the far field boundary and the airfoil. To verify the mesh independence of the flow field obtained with the grid described above, the flow field of the nominal airfoil and that of the airfoil with the mean groove were also computed using a finer grid. The finer grid was obtained by halving each cell of the medium grid in both directions, yielding a grid with 461,796 quadrilateral cells. The lift and drag curves obtained with the two grids were found to differ negligibly, which confirms the suitability of the 115,449-cell grid for the analysis of this study.

The CFD analyses yielding the $c_l(\alpha)$ and $c_d(\alpha)$ curves of the grooved airfoils are fully turbulent, and do not model BL transition. This is because at the selected Reynolds number of 9M, the depth of the considered LE grooves is well above the critical roughness height [24,26]. These grooves trip the laminar boundary layer and trigger by-pass transition in the LE area. Further discussion of this aspect is reported in [24,26]. Conversely, in the case of the nominal NACA 64_3-618 airfoil, two analyses are performed: one with fully turbulent BLs, and one with free BL transition modeled, using the $\gamma - Re_\theta$ SST model. The lift and drag curves obtained with the latter analysis are required to

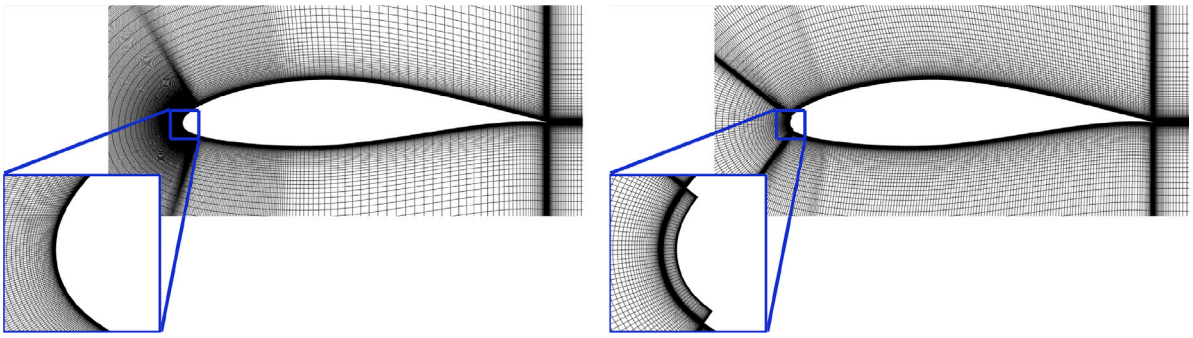

(a) Nominal airfoil. (b) Grooved airfoil.

Fig. 4. Enlarged views of 115,449-cell grids past NACA 64_3-618 airfoil: (a) nominal airfoil geometry and (b) airfoil with mean groove geometry (d/c = 0.4%, s_u/c = 1.9%, s_l/c = 2.47%) at LE.

calculate power and AEP of the reference turbine, needed to measure the reductions of these two outputs for the turbines with damaged blades; the fully turbulent analysis of the nominal airfoil serves two purposes: one is to determine power and AEP losses caused by the loss of BL laminarity due, in turn, to LE roughness levels comparable to the critical roughness height; the other purpose is studying and quantifying blade performance degradation, and turbine power and AEP losses relative to the turbine with larger resolved LEE damage. This result enables the additional loses due to LE geometry perturbations larger than the critical roughness height to be assessed.

The generation of all 343 grooved airfoil grids is fully automated. A single MATLAB code performs a 343-step loop that, at each step, first generates a perturbed variant of the NACA 64_3-618 airfoil, and then launches the grid generator to obtain the grid file. The adopted grid generator is ANSYS ICEM CFD version 21.2 [55].

A fully automated approach is also used to run all 343 CFD analyses yielding the $c_l(\alpha)$ and $c_d(\alpha)$ curves of the grooved NACA 64_3-618 airfoils, with each analysis computing the flow field at 12 values of the AoA, namely for $-8° \leq \alpha \leq 14°$ with step of 2°. At each step of a 343-step loop of a Linux BASH script, a script for each damaged airfoil is submitted to the queue of a computer cluster. Each script has a 12-step loop launching FLUENT for the 12 specified AoA α, using a suitable journal file.

Using one 16-core node of the HEC computer cluster of Lancaster University [56], one CFD simulation using the grid settings reported above requires about 64 min of wall-clock time, and the construction of the lift and drag curves for each grooved airfoil requires about 12 h and 50 min of wall-clock time. Since the database generation is accomplished by using concurrently 21 cluster nodes, the generation of the 343-airfoil force database requires about 210 h of wall-clock time, i.e. about 8.7 days.

4. Airfoil performance sensitivity to groove geometry

This section discusses both the causes of the aerodynamic performance loss due to LE erosion grooves, and the global sensitivity of this loss to the groove geometry. This investigation, in turn, enables explaining the levels and variations of the statistical moments of the turbine power and AEP PDFs of damaged turbines presented in Section 5.

The force coefficients of the nominal airfoil with transitional BLs ('nom. TR.') and fully turbulent BLs ('nom. FT.') are compared with those of airfoil variant labeled 'mean groove', whose damage geometry is defined by the mean values of the first column of Table 1. Figures 5(a), 5(b) and 5(c) report the $c_l(\alpha)$, $c_d(\alpha)$ and efficiency $\varepsilon(\alpha) = c_l/c_d$ curves, respectively. One notes that the loss of BL laminarity of the nominal airfoil results in reduced lift and increased drag, as expected [57,58]. Both the lift reduction and the drag increase are more pronounced at the higher AoAs, but the overall pattern of the $c_l(\alpha)$ and $c_d(\alpha)$ curves are comparable. The relative variations of these curves result in the AoA of maximum efficiency of the nominal fully turbulent airfoil being slightly higher than that of the nominal airfoil with free transition. The lift and drag curves of the grooved airfoil variant differs significantly for level and pattern from those of the nominal airfoils. The peak lift of the eroded airfoil is about 1, whereas, at $\alpha = 14°$, the nominal fully turbulent airfoil has $c_l \approx 1.6$. The drag polar of the grooved airfoil also differs from those of the nominal airfoils, as the former one shows a sudden increase of c_d for $\alpha < -6°$ and $\alpha > 8°$, indicating more abrupt and stronger stall than the nominal airfoils. The aerodynamic efficiency of the grooved airfoil is reduced over that of the nominal airfoils, and the AoA of maximum efficiency decreases slightly with respect to that of the nominal airfoil with free transition.

To investigate the causes of the aerodynamic performance reduction caused by LE grooves, the contour plots of the velocity magnitude and the streamlines past the airfoil featuring the mean groove are reported in Fig. 6. The result refers to $\alpha = 8°$. The view of the flow field past the entire airfoil (right) highlights a stall-induced separation on the airfoil SS in the TE region, with the label 'A' indicating the position of the separation point. At the same AoA, the analysis of the nominal airfoil with fully turbulent BLs, not reported for brevity, predicts a notably smaller separation. The enlarged view of the LE region (left) shows a small separation bubble following the groove edge on the SS. Here, the flow field is similar to that around a forward-facing step on a flat surface. This separation bubble is the key aerodynamic phenomenon accounting for the performance reduction of the grooved airfoils. This LE separation causes the fresh low-momentum SS BL originating at the reattachment point to develop in a region of strong adverse pressure gradient, and this yields earlier stall onset with respect to the nominal airfoil case.

The SS flow separation in the TE region occurs above an airfoil geometry-dependent minimum AoA. Above this threshold, the chordwise position x_A of the separation point depends on the magnitude of the adverse pressure gradient on the airfoil SS, which, in turn, increases with α. This is highlighted in Fig. 7, which plots x_A against α for the nominal airfoil with fully turbulent BLs, and the airfoil with LE mean groove. The LE groove anticipates the onset of stall by about 2° with respect to the nominal airfoil case. As a result, at $\alpha = 14°$, the flow separation covers more than 50% of the grooved airfoil SS, whereas it covers only 30% of the nominal airfoil SS.

The contour plots of Fig. 8 analyze the global sensitivity of the c_l reduction of the grooved airfoils to the three geometry parameters. The considered flow field is that at $\alpha = 6°$, and each contour plot shows the dependence of the c_l reduction on two geometry parameters, keeping the third one constant. The top, middle and bottom subplot rows of Fig. 8 keep, respectively, d/c, s_u/c and s_l/c constant. The constant values of these parameters in the left, middle and right columns are those reported in Table 1. The top row indicates that the c_l reduction is nearly independent of the groove curvilinear extent on the PS, as expected. This is because the loss isolines are almost parallel to the

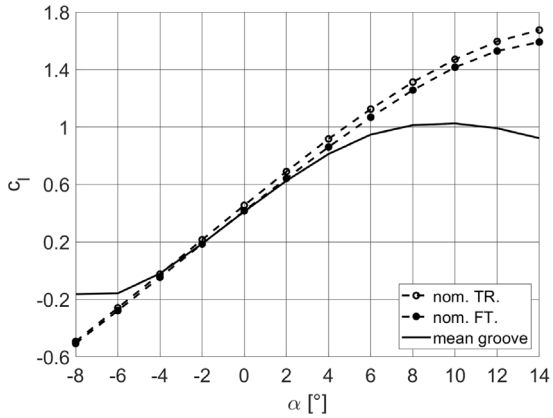

(a) Curves of lift coefficient c_l against AoA α.

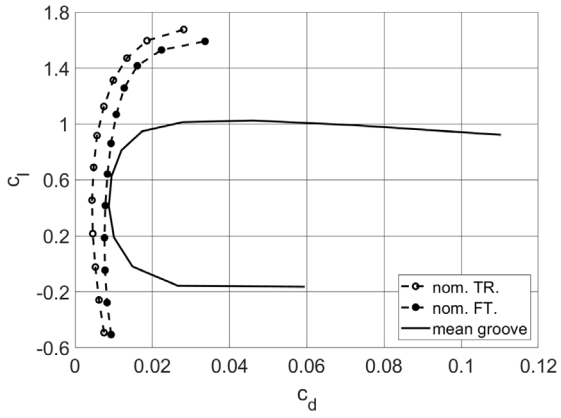

(b) Drag polars.

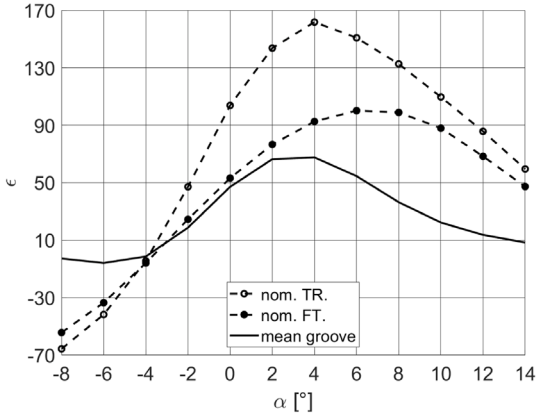

(c) Curves of aerodynamic efficiency $\varepsilon = c_l/c_d$ against AoA α.

Fig. 5. Aerodynamic force coefficients of nominal NACA 64_3-618 airfoil with transitional and fully turbulent BLs, and eroded airfoil with mean groove geometry (d/c = 0.4%, s_u/c = 1.9%, s_l/c = 2.47%) at LE. Results refer to Re = 9M.

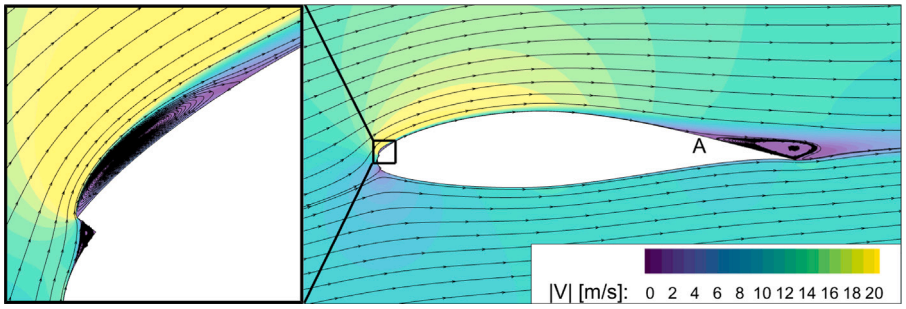

Fig. 6. Velocity magnitude contour plots and streamlines highlighting separation bubble at groove edge (left), and stall-induced TE separation (right) of NACA 64_3-618 airfoil featuring mean groove geometry ($d/c = 0.4\%$, $s_u/c = 1.9\%$, $s_l/c = 2.47\%$) at LE. Results refer to AoA $\alpha = 8°$ and Re = 9M.

s_u/c isolines. Furthermore, the mean value of the aerodynamic loss increases from about 7.4% in the left subplot to about 18.2% in the right subplot, indicating a strong dependence of the performance loss on d/c. The broader color range in the right plot also indicates a stronger dependence of the loss on s_u/c at high values of d/c.

The middle row of subplots, which considers the case in which s_u/c is constant, confirms the weak dependence of the c_l reduction on s_l/c. The left plot of this row also shows an additional feature, namely that, for small values of both s_u/c and s_l/c, there exists a maximum threshold of the groove depth d/c above which the loss is independent of the groove depth. When s_u/c and s_l/c tend to zero, the groove geometry tends to a pit, and the observation above indicates that, in the considered range, the aerodynamic loss is independent of the pit depth. This observation is qualitatively in line with the findings of a parametric 3D analysis of the aerodynamic losses due to erosion cavities [53], which found that the airfoil aerodynamic loss for two depths of a LE cylindrical cavity was the same.

The bottom row of subplots of Fig. 8 confirms a strong dependence of the c_l reduction on both d/c and s_u/c. The strong deviation of the loss isolines from the linear pattern in all three subplots indicates a nonlinear dependence of the loss on the two geometry variables. The dependence of the loss on s_u/c varies from weak, at low values of d/c, to strong at high values of d/c; that on d/c is overall stronger: it is already significant at low values of s_u/c, and it becomes highest at high values of s_u/c, with the loss varying from about 6.9% to about 21.4% as d/c spans its domain of definition.

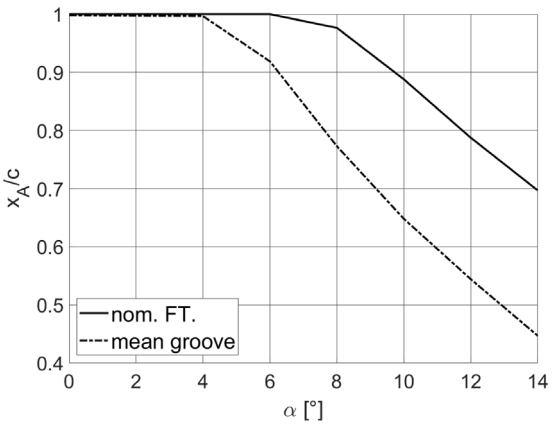

Fig. 7. Dependence of position of TE separation point x_A on AoA α for nominal NACA 64_3-618 airfoil and grooved airfoil variant featuring mean groove geometry ($d/c = 0.4\%$, $s_u/c = 1.9\%$, $s_l/c = 2.47\%$). Both airfoils with fully turbulent BLs. Results refer to Re = 9M.

The contour plots of the c_d increase, and those of the ϵ reduction are not reported for brevity. Their patterns are similar to those of the c_l loss contours, pointing to a similar dependence of all three aerodynamic performance metrics on the geometry parameters of the LE groove.

5. Results

This section discusses several aspects of wind turbine performance degradation due to LEE accounting for uncertainty on some or all of the geometry variables defining the damaged blade geometry. Section 5.1 analyses in a deterministic simplified fashion the sensitivity of the damaged turbine power and AEP to the geometry parameters of the grooved blades. The probabilistic analyses of offshore power output and AEP considering more realistic erosion patterns are reported in Section 5.2. Section 5.3 analyzes the sensitivity of the probabilistic estimates of the turbine performance degradation to different levels of radial resolution of the LE damage geometry. Section 5.4 demonstrates the potential of the URQ UP method for handling LEE geometry uncertainty in probabilistic AEP analyses, and applies a novel statistical method for verifying the AEP standard deviations of the MC analyses. Section 5.5 assesses the impact of uncertain LEE data on onshore turbine power and AEP.

5.1. Power curve and AEP sensitivity to groove geometry

To assess in a deterministic fashion the sensitivity of turbine power and energy yield to the groove geometry, here it is assumed that all 50 strips of the outer 30% of the blade feature the same erosion damage, i.e. the same values of the three groove parameters d/c, s_u/c and s_l/c. The power curves of 343 turbines featuring all possible values of these three parameters, based on the ranges of Table 1, are then computed. The analyses of this section refer to the offshore site. A graphical summary of the computed power curves is provided in Fig. 9. The curve labeled 'P nom. TR.' is the power curve of the turbine with nominal blade geometry and free BL transition. This is the reference power curve for calculating all offshore power and AEP losses of this report. The result of the global sensitivity analysis of the power loss to the groove geometry is represented by the red power loss band in Fig. 9. For each wind speed, the width of the band gives the variability of the power loss of 343 turbines, each using one of the grooved NACA 64_3-618 along the outer 30% of the blade. The upper and lower bounds of the band are the power loss curves of the turbine yielding the lowest and highest AEP, respectively, and the curve of the mean power loss is that of the turbine yielding the mean AEP. These deterministic predictions highlight that the range of power losses associated with the 343 grooves is significant. For example, at 10 m/s the power loss due to the LE grooves may vary between about 2.4 and 8.7%.

The contour plots of Fig. 10 present a global analysis of the dependence of the offshore AEP loss of the wind turbines featuring one of the 343 admissible grooved NACA 64_3-618 airfoils. The three contour plots show the dependence of the AEP loss on d/c and s_u/c for s_l/c set to the minimum, mean and maximum values provided in Table 1. The small differences among the three plots demonstrate a weak dependence of the loss on s_l/c. Conversely, a strong dependence of the AEP loss on d/c and s_u/c is observed. The deviation of the loss isolines from the linear pattern in all three subplots indicates a nonlinear dependence of the loss on these two variables, particularly for high values of both variables. The dependence of the loss on s_u/c varies from weak, at low values of d/c, to strong, at high values of d/c; the dependence of the loss on d/c is overall stronger: it is already significant at low values of s_u/c, and becomes highest at the high values of s_u/c, varying from 1% to 3.7% as d/c spans its domain of definition.

5.2. Probabilistic analysis of offshore power and AEP losses

The deterministic power output of the reference offshore turbine and that of the damaged variants defined below are compared in Fig. 11(a). The curve labeled 'P nom. TR.' is the reference power curve, defined in Section 5.1. The curve labeled 'nom. FT. P loss' is the power loss curve of the turbine with nominal blade geometry and fully turbulent BLs. This configuration is representative of LEE early stages. The probabilistic power loss band associated with the blades affected by uniformly distributed uncertainty of all three groove geometry parameters is obtained as follows. The three groove parameters of the 50 NACA 64_3-618 strips are assumed to vary randomly and independently of each other. Uncertainty is propagated using a 10,000-sample (or 10,000-turbine) MC analysis, as for all MC analyses of this report. The upper and lower bounds of the band are the power loss curves of the turbines yielding the lowest and highest offshore AEP, respectively, and the curve of the mean power loss is that of the turbine yielding the mean AEP.

Inspection of the curves of Fig. 11(a) shows that the power losses due to small erosion levels causing the loss of BL laminarity vary between about 2 and 4% between 6 and 12 m/s. More importantly, between about 8 and 11 m/s, a wind speed range where significant energy amounts are produced, the power loss due to large resolved erosion is at least twice that of the turbine with nominal blade geometry and fully turbulent BLs, taking the lower bound of the loss band as an optimistic loss estimate. This indicates that the power loss due to the aerodynamic perturbations caused by the larger scales of erosion is comparable to that due to the loss of BL laminarity, and underlines the importance of resolving the geometry of erosion in aerodynamic analyses for turbine performance and AEP loss assessments.

It is observed that the wind speed range over which significant power losses by resolved LEE are experienced is similar to that of the case in which the same damage affects all grooved blade sections, analyzed in Fig. 9. However, the width of the power loss band is smaller when the uncertain groove geometry varies independently in the 50 grooved strips. At 10 m/s, power losses vary between 3.8 and 5.7% when the LEE damage varies independently in all 50 blade sections, whereas they vary between 2.4 and 8.7% when the uncertain groove geometry relative to the chord length is the same for all 50 strips. This is because the former, more realistic, damage model results in a given blade featuring sections with varying degree of performance reduction, an occurrence that smoothens rotor power variations. Moreover, the probability that all 50 strips will feature simultaneously the worst or the least severe grooves is insignificant, and this reduces further the scatter of the power loss with respect to the deterministic analysis of Fig. 9.

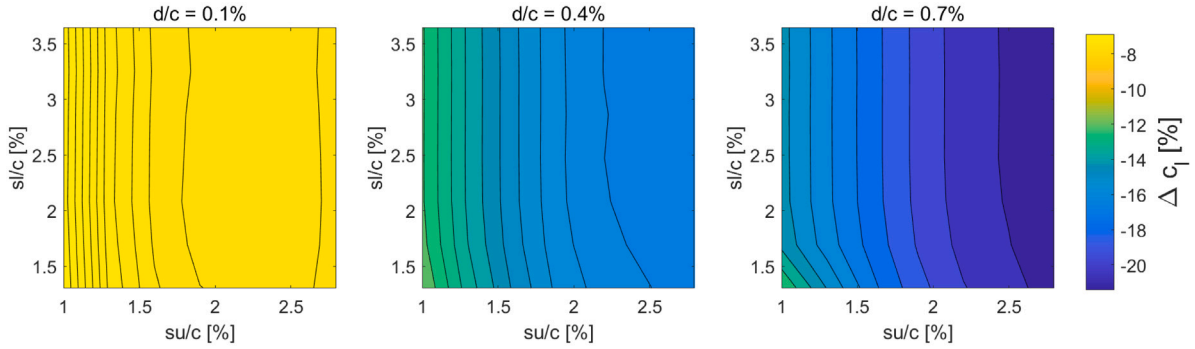

(a) Dependence of c_l reduction on s_u/c and s_l/c keeping d/c at its minimum (left), mean (middle) and maximum (right).

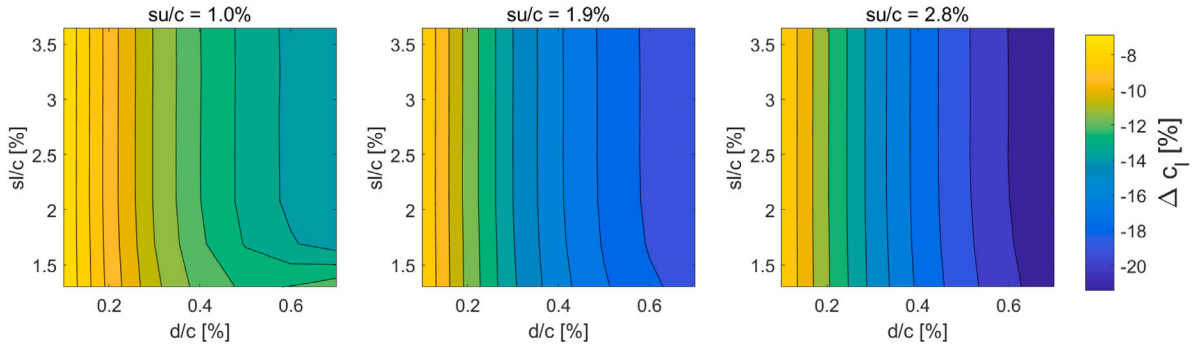

(b) Dependence of c_l reduction on d/c and s_l/c keeping s_u/c at its minimum (left), mean (middle) and maximum (right).

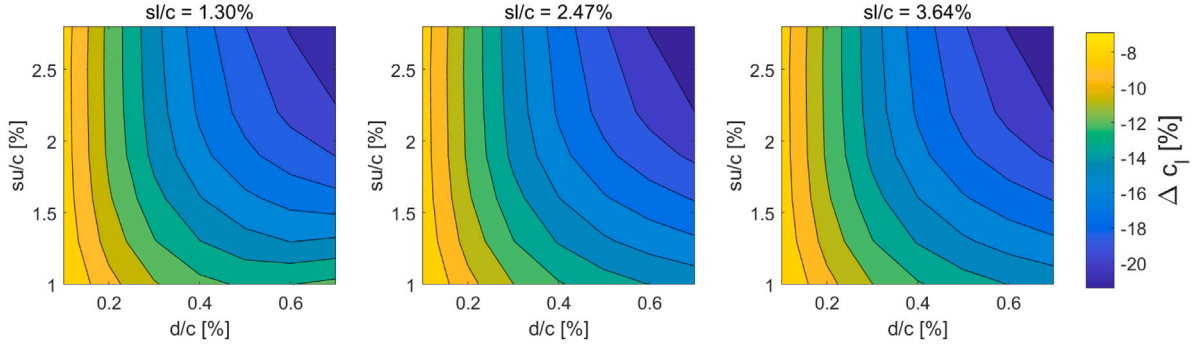

(c) Dependence of c_l reduction on d/c and s_u/c keeping s_l/c at its minimum (left), mean (middle) and maximum (right).

Fig. 8. Percentage reduction of lift coefficient c_l of all grooved variants of NACA 64_3-618 airfoil of analysis space defined in Table 1 over value of nominal airfoil with transitional BLs. Each contour plot reports dependence of c_l reduction on two geometry parameters keeping the third one constant. Results refer to AoA $\alpha = 6°$ and Re = 9M.

The probability histogram of the power loss at 10 m/s, which is part of the results of the 10,000-sample MC analysis varying all three groove parameters, is presented in Fig. 11(b). The figure also reports the mean power loss of about 4.7% at the considered wind speed. It is emphasized that this figure is not the mean value of the 10,000 power loss values, but is the mean power loss of the turbine which yields the mean value of the 10,000 AEP loss estimates. The mean value of the power loss and that reported in Fig. 11(b) are close, but not equal. The standard deviation of the reported data is about 0.23%, and the histogram indicates that the distribution of the power loss is fairly smooth and symmetric.

The main results of the probabilistic assessment of the offshore AEP losses due to uncertain LEE geometry are reported in Fig. 12. All four MC analyses are for the LE groove geometry varying randomly and independently in all 50 blade strips. The probability histogram labeled 'MC_{all}' considers the case in which all three groove parameters are uncertain, and the histogram is thus a scaled representation of a joint AEP PDF. The MC_{all} analysis is representative of the case in which only relatively qualitative data of the LE surface erosion state are available, e.g. photographic footage with incomplete surface dimensions and depth of the erosion patch. The remaining three probability histograms are for the case in which only the relative groove depth d/c is uncertain. The probability histograms '$MC_{s\text{-}min}$', '$MC_{s\text{-}mean}$' and '$MC_{s\text{-}max}$' refer to s_l/c and s_u/c kept to their minimum, mean and maximum values, respectively. These histograms are scaled representations of marginal AEP PDFs. The assessment with uncertainty affecting only the groove depth is also representative of the case in which all erosion geometry parameters are uncertain but the largest uncertainty is that on d/c. These analyses are particularly relevant to future industrial implementations of the presented methods, because erosion depth is difficult to measure in typical blade surface inspections.

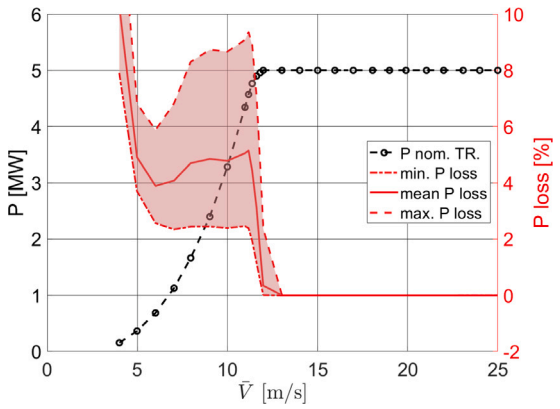

Fig. 9. Power curve of nominal NREL 5 MW turbine and power loss band of 343 damaged turbines featuring same grooved NACA 64_3-618 variant along outer 70%. Results refer to offshore site TI.

Table 2
Deterministic AEP values and mean AEP value corresponding to uncertainty affecting simultaneously all three groove geometry parameters of results in Fig. 12. Standard deviation of MC_{all} and expected AEP losses are also reported. Analysis refers to offshore site.

		nom. TR.	nom. FT.	mn. grv.	MC_{all}
AEP [GWh]	μ	22.22	22.02	21.73	21.77
	σ	–	–	–	$22.4 \cdot 10^{-3}$
	Loss %	–	0.9	2.2	2.0

The AEP of the damaged turbine with all 50 eroded blade sections featuring the mean groove geometry (red line labeled 'mn. grv.') is also reported in Fig. 12, along with the AEP of the reference turbine ('nom. TR.'), and that of the nominal turbine with fully turbulent BLs ('nom. FT.'). Comparing the mean AEP of the MC_{all} histogram with the reference AEP, shows that the mean AEP loss when all three groove geometry variables are uncertain is about 2%. The minimum and maximum AEP of the MC_{all} histogram are close to each other, indicating a small AEP standard deviation, notwithstanding the relatively large uncertainty intervals of the three LE groove parameters. This is in line with the small width of the probabilistic power loss band shown in Fig. 11(a). The reason for the small variability of the power and AEP losses is discussed in Section 5.3.

One notes that the mean AEP of the MC_{all} analysis differs from the AEP corresponding to the mean groove geometry applied to all 50 NACA 64_3-618 strips. This is due to the nonlinear dependence of AEP on d/c and s_u/c, highlighted in Fig. 10. This nonlinearity causes the region of the analysis domain where the AEP is higher to outweigh that where losses are higher. Thus, averaging over the entire domain yields a mean AEP loss which is smaller than the AEP evaluated at the mean values of all three perturbations. The variability range of the damage parameters used in this study are deliberately fairly large to test for significant geometry uncertainty. Reducing the width of these intervals would result in the difference between these two values tending to zero. The geometry uncertainty and the corresponding damage parameter variability depends on the quality of the available field records.

It is also seen that the mean AEP loss corresponding to the difference between the AEP of the reference turbine and the mean AEP of the MC_{all} analysis is more than twice that due to the loss of BL laminarity, which is only 0.9%. Once again, this emphasizes the importance of resolving the larger scales of LEE.

The AEP values and losses, along with the standard deviation of the MC_{all} analysis are reported in Table 2. The loss standard deviation of the MC_{all} analysis is very small, amounting to about 0.1% of the mean AEP. This is a positive outcome with regard to the future use of field records of blade LEE in predictive maintenance, since it indicates that relatively wide uncertainty ranges of the damage parameters will not prevent obtaining mean AEP losses affected by small uncertainty. This conclusion may be influenced by other factors, such as the resolution of the damage geometry along the damaged blade length, an aspect analyzed in Section 5.3. The data of Table 2 also show that the difference between the AEP loss of the turbine with mean LE groove along the entire damaged blade patch, and the mean AEP is only 0.2%. This indicates that a good initial estimate of the AEP loss may be rapidly obtained when reliable estimates of the mean damage are available.

Table 3
Nominal AEP value and mean AEP values corresponding to uncertainty affecting groove geometry parameter d/c at three constant values of the other two geometry parameters of results in Fig. 12. Standard deviation of all three MC analyses and expected AEP losses are also reported. Analysis refers to offshore site.

		nom. TR.	$MC_{s\text{-}mean}$	$MC_{s\text{-}min}$	$MC_{s\text{-}max}$
AEP [GWh]	μ	22.22	21.75	21.91	21.67
	σ	–	$20.2 \cdot 10^{-3}$	$6.3 \cdot 10^{-3}$	$28.7 \cdot 10^{-3}$
	Loss %	–	2.1	1.4	2.5

The values of the AEP mean and standard deviation of the $MC_{s\text{-}min}$, $MC_{s\text{-}mean}$ and $MC_{s\text{-}max}$ analyses are reported in Table 3, along with the expectation of the corresponding AEP losses. These data show that, for the considered ranges of the groove geometry parameters, the mean AEP loss due to uncertainty on d/c varies between 1.4 and 2.5% of the reference AEP, with the AEP loss corresponding to the mean values of s_u/c and s_l/c being 2.1%. The AEP standard deviations in the three cases are small, with the maximum being only 0.13% of the corresponding mean AEP. The mean values and widths of the three AEP probability histograms of Fig. 12 for uncertainty affecting only d/c are also consistent with the AEP contour plots of Fig. 10. When s_u/c is set to its minimum value, the expected value of the AEP loss is the smallest of the three cases, and the standard deviation is very small, in line with the fact that the dependence of AEP on d/c is weak, and the AEP loss range for d/c varying between its maximum and minimum is small. When s_u/c takes its mean value, both the expected value and the standard deviation of the AEP loss are close to those of the MC_{all} analysis. When s_u/c equals its maximum value, the expectation of the AEP loss is the largest of the three cases, and the standard deviation is also maximum, in line with the fact that the dependence of AEP on d/c is strong, and the AEP loss range for d/c varying between its maximum and minimum is significant.

All 10,000-sample MC analyses were run using concurrently 350 processors of Lancaster University's HEC cluster. The elapsed wall-clock time for each MC simulation using this set-up was about 7.5 days.

5.3. Probabilistic sensitivity of offshore AEP loss to LEE radial resolution

This section investigates the probabilistic dependence of the offshore AEP loss on the radial resolution of the geometry perturbations due to LEE. To this end, the 50 blade strips of the damaged blade portion are grouped in sets of adjacent strips, with the airfoils of each set featuring the same percentage value of d/c, s_u/c and s_l/c). The problems named 'MC_{all} - 10s' and 'MC_{all} - 5s' are those using 10 and 5 strip sets, respectively. The problem named 'MC_{all} - 50s' is that in which the damage geometry varies independently in all 50 strips, already examined in the previous subsection. The radial length of each strip of the 'MC_{all} - 50s', 'MC_{all} - 10s' and 'MC_{all} - 5s' set-ups are 0.378 m, 1.890 m and 3.780 m, respectively.

The findings of this analysis are presented in Fig. 13, which presents the results of the MC sampling as discrete PDFs, rather than probability histograms. The reason for choosing the PDF representation is only that this scaling enables a simpler graphical representation of all three results. One observes that all three probabilistic analyses predict the same AEP expectation of about 21.77 GWh, and the same loss expectation of about 2.0%. However, the AEP standard deviation

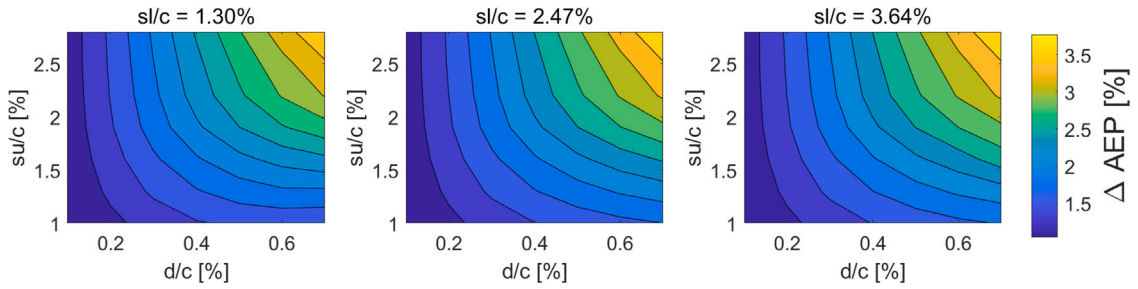

Fig. 10. Offshore AEP loss of NREL 5 MW turbine with outer 30% of blades featuring NACA 64_3-618 grooved airfoil variants with constant groove geometry parameters (for each turbine) spanning entire analysis space defined in Table 1. AEP loss computed with respect to offshore AEP of turbine with nominal blade geometry and transitional BLs. Contour plot show dependence of AEP loss on d/c and s_u/c keeping s_l/c at its minimum (left), mean (middle) and maximum (right).

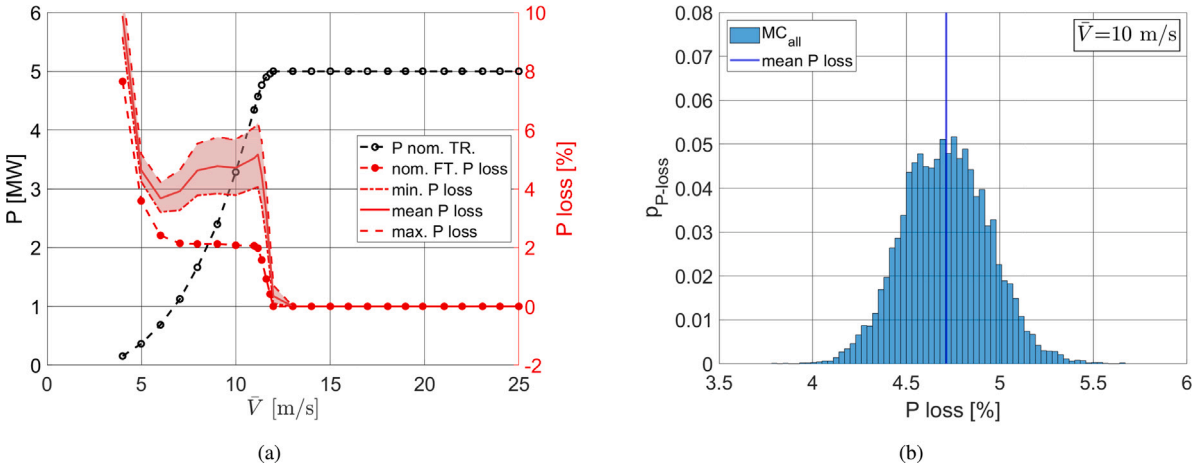

Fig. 11. Left: power curve of nominal NREL 5 MW turbine and probabilistic power loss band associated with blades affected by uniformly distributed uncertainty on groove geometry parameters. Power loss curve of turbine with nominal blades and fully turbulent BLs is also reported. Right: probability histogram of power loss at mean wind speed of 10 m/s. Damaged blades feature grooved NACA 64_3-618 variants along outer 70%, with geometry parameters ranges given in Table 1. MC sampling is used for uncertainty propagation, and results refer to offshore site TI.

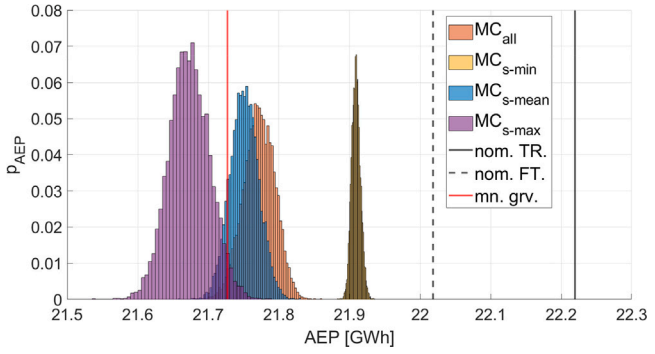

Fig. 12. Offshore AEP probability histograms of turbines considering uncertain LE erosion groove geometry and using MC sampling for uncertainty propagation. Probabilistic analyses consider uncertainty on both all three groove geometry parameters simultaneously and d/c in isolation. Deterministic values of turbines with blades having mean groove damage applied to all NACA 64_3-618 airfoils, and with nominal blade geometry featuring transitional and fully turbulent BLs are also reported.

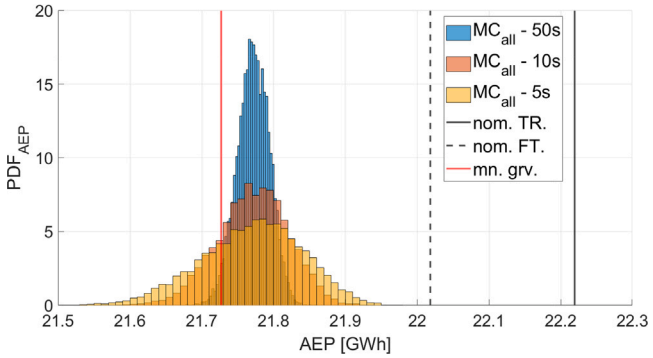

Fig. 13. Discrete MC-based AEP PDFs of turbines at offshore site considering uncertain LE erosion groove geometry. Three PDFs differ for radial length of set of adjacent strips featuring the same percentage values of the damage parameters. Deterministic values of turbines with blades having mean groove damage applied to all NACA 64_3-618 airfoils, and with nominal blade geometry featuring transitional and fully turbulent BLs are also reported.

varies significantly, amounting to 22.40, 49.29 and 70.14 MWh for the number of damaged strips equal to 50, 10 and 5, respectively. The computed AEP standard deviations correspond to 0.10, 0.23 and 0.32% of the AEP expectation. The reduction of the AEP standard deviation as the radial resolution of the LE damage increases is due to the balance of larger and smaller negative contributions to the overall AEP increasing as the LE damage variability increases. This result is quite relevant for perspective predictive maintenance, because it highlights that, in the realistic case of distributed LE damage, varying with a radial step of about 40 cm (in the considered example) or less, the standard deviation of the AEP loss is substantially smaller than its expectation. Therefore, reasonably reliable estimates of the minimum and maximum values of

Table 4
URQ AEP mean and standard deviation, first four MC AEP moments, and AEP standard deviation of the fitted beta distribution method. distributions for the probabilistic turbine performance assessment with different radial resolution levels of LEE geometry.

	URQ		MC_{all}				β
	μ [GWh]	σ [GWh]	μ [GWh]	σ [GWh]	γ_s [–]	Γ_K [–]	σ [GWh]
50 s	21.77	$21.1 \cdot 10^{-3}$	21.77	$22.4 \cdot 10^{-3}$	−0.146	2.97	$23.1 \cdot 10^{-3}$
10 s	21.77	$45.8 \cdot 10^{-3}$	21.77	$49.3 \cdot 10^{-3}$	−0.201	2.95	$47.0 \cdot 10^{-3}$
5 s	21.77	$63.9 \cdot 10^{-3}$	21.77	$70.1 \cdot 10^{-3}$	−0.287	2.89	$79.3 \cdot 10^{-3}$

the geometry damage parameters will enable a reliable prediction of mean turbine power and AEP losses.

5.4. Univariate reduced quadrature UP method and verification of Monte Carlo UP set-up

The deterministic derivative-free URQ UP method [33], initially developed for robust design optimization in aeronautics, and successively used in other engineering areas, including the robust design optimization of stall regulated turbines accounting for blade shape uncertainty due to manufacturing and assembly tolerances [59], has been applied also to the analysis of the three probabilistic problems considered in Section 5.3. URQ enables calculating expectation and standard deviation of a function depending on N_v independent variables affected by uncertainty, requiring the mean, standard deviation, skewness and Kurtosis of the PDFs of the N_v variables. These four statistical moments can all be determined in the present case of uniformly distributed uncertainty. The URQ expectation and standard deviation are then computed using $2N_v + 1$ predefined perturbations of the input variables. The values of N_v for the probabilistic wind turbine problems considering independent groove geometry for 50, 10 and 5 blade strips are 150, 30 and 15, respectively. For these three cases, therefore, URQ requires calculating the AEP of 301, 61 and 31 perturbed turbines, respectively. By contrast, all MC_{all} analyses herein require calculating the AEP of 10,000 turbines.

The URQ mean and standard deviation for these three problems are reported in the first and second column of Table 4, respectively, whereas the MC_{all} estimates of these two moments are reported in the third and fourth columns. The URQ and MC_{all} estimates of the mean AEP values are equal. The standard deviations predicted by the two methods are in fairly good agreement, and the two methods predict the same trend of growing AEP standard deviation as the radial resolution of the LE damage decreases. In addition to providing a verification of the MC_{all} analyses, these results also demonstrate a viable means of deploying the presented probabilistic ALPS framework in future industry applications, since the computational cost of one URQ analysis is at least 30 times smaller than that of the MC analysis, thus greatly reducing run-rimes. The fifth and sixth columns of Table 4 also report the skewness γ_s and the Kurtosis Γ_K of the three MC-based AEP PDFs depicted in Fig. 13. The γ_s and Γ_K data of the table show in a quantitative manner the rate by which the AEP PDF deviates increasingly from a symmetric shape as the radial resolution of the LE perturbations decreases.

All results discussed so far indicate that the AEP standard deviation accounting for uncertainty on the LEE geometry is fairly small, notwithstanding the relatively wide uncertain geometry ranges considered. In order to further verify the reliability of this outcome and the discussed trends of the AEP standard deviations obtained with the MC and URQ UP methods, an alternative approach for determining the AEP standard deviation is proposed. The method relies on fitting the AEP PDF obtained with MC sampling to a beta distribution function [60], whose expression is:

$$p_\beta(x,a,b) = \frac{\Gamma(a)\Gamma(b)}{\Gamma(a+b)} x^{a-1}(1-x)^{b-1} \tag{3}$$

The function p_β has support [0,1], the parameters a and b are positive real numbers, and Γ denotes the gamma function. The reason for selecting the beta function is that it has a finite support, which is known to be the case also for the true AEP PDFs. This is because the tails of the true AEP PDFs are finite, with the maximum AEP (AEP_{max}) of 21 988 MWh and the minimum AEP (AEP_{min}) of 21 382 MWh corresponding, respectively, to the minimum and maximum possible values of the three damage parameters for all 50 damaged blade sections. Moreover, it is known from the results of the present investigation and previous others [31,32], that the AEP PDF is not symmetric, and this feature is captured by the beta distributions when $a \neq b$.

The two conditions imposed for the beta fitting are that the mean value and the median of the MC-based AEP PDF be equal to those of the fitting beta distribution. These two conditions yield, respectively, Eqs. (4) and (5), whose coupled solution provides the values of a and b defining the fitting beta distribution.

$$\mu'_\beta = \frac{a}{a+b} \tag{4}$$

$$\int_0^{M'} p_\beta(x,a,b)dx = 0.5 \tag{5}$$

The symbol μ'_β denotes the mean AEP μ of the MC PDF referred to the support of the beta distribution, i.e. $\mu'_\beta = (\mu - AEP_{min})/(AEP_{max} - AEP_{min})$, and M' denotes the median of the same PDF referred to the support of the beta distribution by means of the same transformation used for the mean value. Once the parameters a and b have been determined, the standard deviation σ'_β of the normalized beta distribution is determined using Eq. (6), and the sought estimate of the AEP standard deviation is $\sigma_\beta = \sigma'_\beta(AEP_{max} - AEP_{min})$.

$$\sigma'^2_\beta = \frac{ab}{(a+b)^2(a+b+1)} \tag{6}$$

The standard deviation σ_β of the fitted beta distribution for the three cases is shown in the seventh column of Table 4. Good overall agreement of these estimates of the standard deviations and the values predicted by the MC and URQ UP methods is observed, providing further confidence in the outcome of the presented analyses.

5.5. Probabilistic analysis of onshore power and AEP losses

This section provides probabilistic MC-based power and AEP loss analyses for the NREL 5 MW turbine operating at the reference onshore site defined in Section 2. These investigations are performed to evaluate the influence of the site conditions on the probabilistic power and AEP losses caused by the given uncertain LEE geometry.

The probabilistic power loss band of the NREL 5 MW turbine operating at the onshore site and affected by the same uniformly distributed uncertainty of all three groove parameters considered in the offshore case is provided in Fig. 14(a). The three groove parameters vary independently of each other in all 50 damaged blade sections, and uncertainty is propagated using a 10,000-sample MC analysis. The power curve of the onshore reference turbine and the power loss curve of the turbine with nominal blades and fully turbulent BLs are also reported. The generation of all power data of Fig. 14(a) differs from that of their offshore counterpart for the TI levels and the wind shear used in TurbSim. The upper and lower bounds of the loss band refer to the turbines yielding the lowest and highest AEP, respectively, and the mean power loss is that of the turbine yielding mean AEP. Comparing the power loss bands of Figs. 14(a) and 11(a) reveals that the onshore power loss is overall higher than the offshore loss. For example, at 9 m/s the maximum power losses in the onshore and offshore cases are, respectively, 7.0 and 5.8% of the respective nominal power. Furthermore, in the onshore case, power losses occur up to a wind speed which is higher than that at which the power loss of the offshore turbine vanishes. These phenomena occur because the

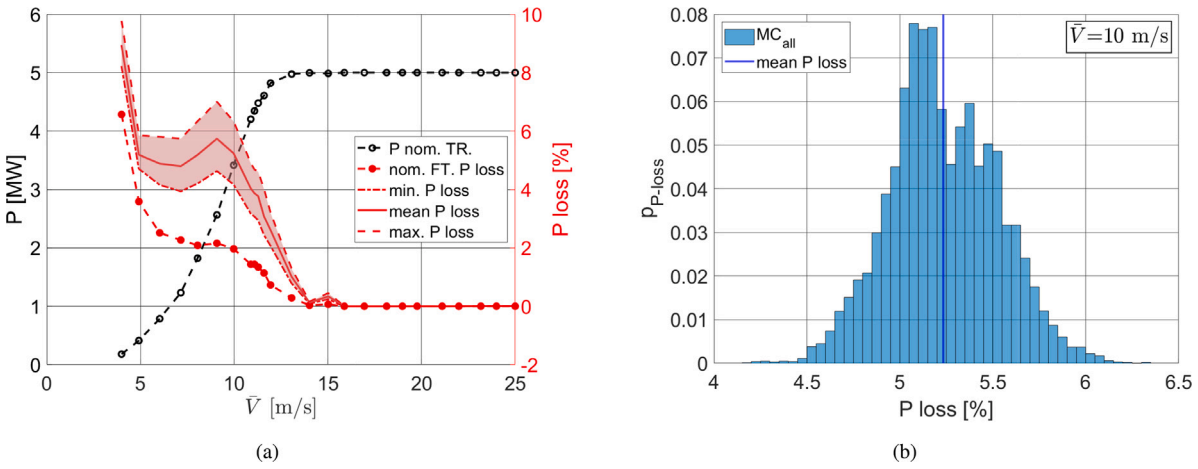

Fig. 14. Left: power curve of nominal NREL 5 MW turbine and probabilistic power loss band associated with blades affected by uniformly distributed uncertainty on groove geometry parameters. Power loss curve of turbine with nominal blades and fully turbulent BLs is also reported. Right: probability histogram of power loss at mean wind speed of 10 m/s. Damaged blades feature grooved NACA 64_3-618 variants along outer 70%, with geometry parameters ranges given in Table 1. MC sampling is used for uncertainty propagation, and results refer to onshore site TI.

higher TI of the onshore site, which leads to increased power at low wind speeds and reduced power at high wind speeds [61], affects to a different extent the nominal turbine and those with LE damage. More specifically, the power of the damaged turbines increases less than that of the nominal turbine at low wind speeds, and decreases more at higher speeds, resulting in the overall onshore power losses being larger than the offshore losses. The power reduction due to the loss of BL laminarity also extends over a slightly wider range of wind speeds than in the offshore case, but the overall loss does not change significantly. Similarly to the offshore case, the loss component due to geometrically resolved erosion is larger than that due to the complete absence of BL laminarity, even when the smallest probabilistic power loss of the eroded turbine loss band is assumed.

The probability histogram of the power loss at 10 m/s is provided in Fig. 14(b). The figure also reports the mean power loss of about 5.2% at the considered wind speed. The standard deviation of the probabilistic data is 0.29%, and the histogram indicates that the distribution of the power loss is fairly smooth, without significant deviations from a symmetric shape.

The outcome of the probabilistic analysis of the AEP losses due to uncertain LEE geometry are reported in Fig. 15. All MC analyses assume that the LE groove geometry varies randomly and independently in all 50 blade strips. The four probability histograms are obtained by using the same methodology used for their offshore counterparts in Fig. 12, i.e. keeping constant and/or MC-sampling the same groove geometry variables. The AEP of the blades with mean groove geometry is also reported, along with the AEPs of the onshore reference turbine and the turbine with nominal blades with fully turbulent BLs. These results show that the onshore AEP level is notably lower than the offshore one, as expected, due primarily to the lower mean wind speed in the former case. The mean AEP loss when all three groove variables are uncertain (MC_{all} analysis) is about 3% of the reference onshore AEP. This loss is 50% higher than that offshore, and the reason for this is two-fold: on one hand, the onshore turbine produces more of its overall AEP below rated wind speed conditions. Thus, for a given power reduction below rated speed, the turbine AEP loss increases as the mean wind speed of the site decreases [26]. On the other hand, the larger power loss below rated wind speed of the damaged onshore turbine, relative to its offshore counterpart, further penalizes the onshore AEP. Analyses conducted to quantify the role of TI and mean wind speed on the increase of the onshore AEP loss, not reported for brevity, indicate that about 50% of the overall AEP loss increase is caused by the higher TI of the onshore site.

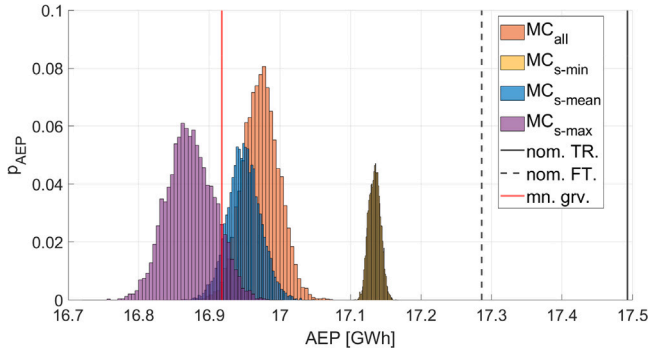

Fig. 15. Onshore AEP probability histograms of turbines considering uncertain LE erosion groove geometry and using MC sampling for uncertainty propagation. Probabilistic analyses consider uncertainty on both all three groove geometry parameters simultaneously and d/c in isolation. Deterministic values of turbines with blades having mean groove damage applied to all NACA 64-618 airfoils, and with nominal blade geometry featuring transitional and fully turbulent BLs are also reported.

The deviation of the mean AEP of the MC_{all} analysis from the AEP corresponding to the blades featuring the same mean groove along their damaged portion is found also in the onshore analysis of Fig. 15. This deviation is caused by the nonlinear dependence of AEP on d/c and s_u/c, discussed in Fig. 10 for the offshore site. These contours are very similar to those of the onshore case, although the range of the onshore AEP loss contours is broader.

The onshore AEP values and losses of the analyses above, along with the standard deviation of the MC_{all} assessment, are reported in Table 5. The mean AEP loss predicted by the MC_{all} analysis, accounting for both the loss of BL laminarity and the probabilistic aerodynamic performance loss due to LEE, and the AEP loss of the 'nom. FT.' analysis, accounting only for the loss of BL laminarity, are 3.0% and 1.1%, respectively. The corresponding offshore values of Table 2 are 2% and 0.9%, respectively. These data indicate a comparable AEP loss due to the lack of BL laminarity for the offshore and onshore turbines; they also highlight that the mean AEP loss due to the LE damage of the onshore case is about twice that of the offshore case. This is in line with the fact that the power loss of the onshore turbine due to fully turbulent BLs (Fig. 14(a)) is comparable to that of the offshore turbine (Fig. 11(a)), whereas the level of the overall power loss due to fully turbulent BLs and LE grooves is significantly higher for the onshore turbine. These results confirm that, for the onshore

Table 5
Deterministic AEP values and mean AEP value corresponding to uncertainty affecting simultaneously all three groove geometry parameters of results in Fig. 15. Standard deviation of MC_{all} and expected AEP losses are also reported. Analysis refers to onshore site.

		nom. TR.	nom. FT.	mn. grv.	MC_{all}
AEP [GWh]	μ	17.49	17.29	16.92	16.97
	σ	–	–	–	$25.6 \cdot 10^{-3}$
	Loss %	–	1.1	3.3	3.0

Table 6
Nominal AEP value and mean AEP values corresponding to uncertainty affecting groove geometry parameter d/c at three constant values of the other two geometry parameters of results in Fig. 15. Standard deviation of all three MC analyses and expected AEP losses are also reported. Analysis refers to onshore site.

		nom. TR.	$MC_{s\text{-}mean}$	$MC_{s\text{-}min}$	$MC_{s\text{-}max}$
AEP [GWh]	μ	17.49	16.95	17.13	16.87
	σ	–	$23.3 \cdot 10^{-3}$	$8.3 \cdot 10^{-3}$	$33.4 \cdot 10^{-3}$
	Loss %	–	3.1	2.1	3.5

and offshore conditions, and the considered uncertain LEE damage, the higher TI of the onshore site plays a key role in increasing the AEP loss of the eroded turbine at the onshore site. The standard deviation of the onshore MC_{all} analysis in Table 5 amounts to about 0.15% of the mean AEP, indicating a narrow range of loss variability, similarly to the offshore case.

The mean values and widths of the three AEP probability histograms of Fig. 15, considering uncertainty affecting only the groove depth, show the same trends of the offshore case. When s_u/c is minimum, the expected value of the AEP loss is the smallest of the three cases, and the histogram spread, a measure of the AEP standard deviation, is very small, although slightly wider than in the offshore case. When s_u/c takes its mean value, both the expected value of the AEP loss and its standard deviation are close to those of the MC_{all} analysis. When s_u/c is maximum, the expected AEP loss is the largest of the three cases, and the histogram spread is also maximum. The values of the AEP expectations and standard deviations of these three MC analyses are reported in Table 6, along with the expectation of the corresponding AEP losses. These data show that, for the considered LE damage geometry ranges, the mean AEP loss varies between 2.1 and 3.5% due to uncertainty on d/c, with the AEP loss corresponding to the mean values of s_u and s_l being 3.1%. The AEP standard deviations in the three cases are small, with the maximum being about 0.20% of the corresponding mean AEP.

6. Conclusions

The article presented an assessment of the probabilistic variability of the power and energy yield loss of a 5 MW wind turbine due to uncertain field records of LEE geometry, for operation at a North Sea offshore site and a southern European onshore site. Overall, the standard deviations of power and energy yield degradation are relatively small, notwithstanding the relatively large uncertainty levels of the LEE geometry. The high radial frequency of the LE damage, typical of moderate to severe LEE often observed in operation, contributes significantly to this outcome.

Most probabilistic performance assessments were performed using 10,000-turbine MC analyses, whereby each sample consisted of a turbulent wind ALPS analysis of a damaged turbine. Assuming the LE damage to affect the outer 30% of the blade, described by 50 geometrically independent strips measuring about 40 cm radially, and considering fairly wide ranges of uniformly distributed uncertainty of the erosion geometry parameters, the mean offshore AEP loss was found to be 2.0%, with a small standard deviation of about 0.1% of the expected value. The mean AEP loss was found to be independent of the radial width of the grooved blade strips.

The AEP standard deviation was found to increase as the radial width of each strip increased above 40 cm. This effect is due to the balance of lower and higher aerodynamic losses increasing as the radial variability of the damage increases. This effect reduces the uncertainty on performance and energy yield loss, since real distributed LEE damages feature geometry perturbations which vary in less than 40 cm radial length, resulting in small standard deviations of the AEP loss, and, thus, high probability of loss values around the mean.

The power and AEP loss trends at the onshore site were found to be similar to those at the offshore site. The same uncertain LEE damage of the offshore analysis, yielded mean onshore AEP loss of 3.0%, 50% larger than the offshore AEP loss. The standard deviation of the AEP loss also increased by about 50% over the offshore case. The higher AEP loss at the onshore site was found to be caused by both the lower mean wind speed, and the higher turbulence intensity onshore, with both factors accounting for about 50% of the increased AEP loss. A key novel finding is that, as the site freestream TI increases, the overall power reduction of the turbine with severe LEE grows more rapidly than that of the turbine with lower LEE levels, which lead only to loss of BL laminarity, without changing significantly the nominal blade geometry. Thus, the onshore and offshore deterministic AEP losses due to the lack of BL laminarity of the nominal blades differ by about 22%, whereas the higher onshore and offshore probabilistic AEP losses due to more severe LEE differ by 50%.

The deterministic derivative-free URQ UP approach yielded estimates of the AEP mean and standard deviation in good agreement with the predictions of the MC analyses, at a computational cost at least 30 times smaller.

The findings of the presented investigations strengthen the prospects of blade predictive maintenance. With regard to blade surface repairs, this approach is presently hindered by the difficulty of acquiring with sufficient resolution the damaged LE state, which, in turn, makes it difficult to quantify the AEP revenue loss. The presented probabilistic analysis framework, based on the LE groove model, shows that the mean AEP loss is fairly independent of the radial resolution adopted in the analysis, indicating that reasonable estimates of mean performance and AEP losses may be obtained by only acquiring either the minimum and maximum values of all LEE geometry parameters, or just their mean values. The fact that the high radial frequency of real moderate to severe erosion results in low standard deviation of the AEP loss, reduces the uncertainty on the AEP loss costs, thus reducing uncertainty in the cost analyses required for predictive maintenance. Furthermore, the high execution speed of the URQ approach to uncertainty propagation makes the presented probabilistic framework routinely usable for robust wind farm O&M cost management.

Future work includes confirming the findings of the presented study for more general LEE geometries acquired from field inspections, accounting for the inherently multi-scale nature of eroded LE geometries, and including in the probabilistic analysis the dependence of the mean erosion state on the local radius of the blade.

CRediT authorship contribution statement

M. Sergio Campobasso: Conceptualization, Formal analysis, Funding acquisition, Investigation, Methodology, Project administration, Resources, Supervision, Writing – review & editing. **Alessio Castorrini:** Data curation, Formal analysis, Investigation, Methodology, Supervision, Validation, Visualization. **Andrea Ortolani:** Data curation, Investigation, Methodology, Validation, Visualization. **Edmondo Minisci:** Methodology, Data curation.

Declaration of competing interest

The authors declare that they have no known competing financial interests or personal relationships that could have appeared to influence the work reported in this paper.

Data availability

Data will be made available on request.

Acknowledgments

All CFD simulations herein were performed on Lancaster University's HEC cluster. The project was supported by the UK Engineering and Physical Sciences Research Council, Grant No. EP/R511560/1, and HeliSpeed Ltd, whose initiatives in wind turbine condition monitoring prompted this research programme.

References

[1] Wood RJK, Lu P. Leading edge topography of blades–a critical review. Surf Topogr: Metrol Prop 2021;9:023001.
[2] Gao L, Tao T, Liu Y, Hu H. A field study of ice accretion and its effects on the power production of utility-scale wind turbines. Renew Energy 2021;167:917–28.
[3] Caccia F, Guardone A. Numerical simulation of ice accretion on wind turbine blades. Wind Energy Sci Discuss 2022;2022:1–27.
[4] Khalfallah MG, Koliub AM. Effect of dust on the performance of wind turbines. Desalination 2007;209:209–20.
[5] Corten GP, Veldcamp HF. Aerodynamics: Insects can halve wind-turbine powers. Nat Brief Commun 2001;412:41–2.
[6] Walker J, Green R, Gillies E, Phillips C. The effect of a barnacle-shaped excrescence on the hydrodynamic performance of a tidal turbine blade section. Ocean Eng 2020;217:107849.
[7] Song S, Shi W, Demirel YK, Atlar M. The effect of biofouling on the tidal turbine performance. In: Applied energy symposium. Cambridge, MA, USA: Massachusetts Institute of Technology; 2019.
[8] Farkas A, Degiuli N, Martić I, Barbarić M, Guzović Z. The impact of biofilm on marine current turbine performance. Renew Energy 2022;190:584–95.
[9] Mishnaevsky L, Hasager CB, Bak C, Tilg A-M, Bech JI, Doagou Rad S, Fæster S. Leading edge erosion of wind turbine blades: Understanding, prevention and protection. Renew Energy 2021;169:953–69.
[10] Macdonald H, Infirld D, Nash F, Stack M. Mapping hail meteorological observations for prediction of erosion in wind turbines. Wind Energy 2016;19:777–84.
[11] Ning A, Dykes. Understanding the benefits and limitations of increasing maximum rotor tip speed for utility-scale wind turbines. J Phys Conf Ser 2014;524:012087.
[12] Herring R, Dyer K, Martin F, Ward C. The increasing importance of leading edge erosion and a review of existing protection solutions. Renew Sustain Energy Rev 2019;115:109382.
[13] Mishnaevsky L, Bendixen B, Mahajan P, Fæster S, Johansen NF-J, Paul D, Fraisse A. Repair of wind turbine blades: Costs and quality. J Phys Conf Ser 2022;2265:032032.
[14] RE News. London array braced for blade fix. 2018, renews.biz/110465/%20london-array-braced-for-blade-%EF%AC%81x. Accessed on 28 November 2022.
[15] RE News. Anholt grapples with blade fix. 2018, renews.biz/110279/anholtgrapples-with-blade-%EF%AC%81x. Accessed on 28 November 2022.
[16] Schlichting H, Gersten K. Boundary-layer theory. 9th ed.. London: Springer; 2017.
[17] Schlichting H. Experimentelle untersuchungen zum Rauhigkeitsproblem. Ingenieur - Arch 1936;7:1–34, English translation: 1937. Experimental investigation of the problem of surface roughness. NACA TM 823.
[18] Dalili N, Edrisy A, Carriveau R. A review of surface engineering issues critical to wind turbine performance. Renew Sustain Energy Rev 2009;13:428–38.
[19] Rempel L. Rotor blade leading edge erosion-real life experience. Wind Syst Mag 2012.
[20] Springer GS, Yang C-I, Larsen PS. Analysis of rain erosion of coated materials. J Compos Mater 1974;8:229–52.
[21] Bartolome L, Teuwen J. Prospective challenges in the experimentation of the rain erosion on the leading edge of wind turbine blades. Wind Energy 2019;22:140–51. http://dx.doi.org/10.1002/we.2272.
[22] van Rooij RPJOM, Timmer WA. Roughness sensitivity considerations for thick rotor blade airfoils. J Solar Energy Eng 2003;125.
[23] Chedevergne F. Analytical wall function including roughness corrections. Int J Heat Fluid Flow 2018;73:258–69.
[24] Ortolani A, Castorrini A, Campobasso M. Multi-scale navier-stokes analysis of geometrically resolved erosion of wind turbine blade leading edges. J Phys Conf Ser 2022;2265:032102.
[25] Gaudern D. A practical study of the aerodynamic impact of wind turbine blade leading edge erosion. J Phys Conf Ser 2014;524:012031.
[26] Cappugi L, Castorrini A, Bonfiglioli A, Minisci E, Campobasso M. Machine learning-enabled prediction of wind turbine energy yield losses due to general blade leading edge erosion. Energy Convers Manage 2021;245:114567.
[27] Maniaci D, White E, Wilcox B, Langel C, van Dam C, Paquette J. Experimental measurement and CFD model development of thick wind turbine airfoils with leading edge erosion. J Phys Conf Ser 2016;753:022013.
[28] Shihavuddin A, Chen X, Fedorov V, Nymark Christensen A, Andre Brogaard Riis N, Branner K, Bjorholm Dahl A, Reinhold Paulsen R. Wind turbine surface damage detection by deep learning aided drone inspection analysis. Energies 2019;12.
[29] Durdevic P, Ortiz Arroyo D, Yang Z. Lidar assisted camera inspection of wind turbines - experimental study. In: 1st international conference on electrical, control and instrumentation engineering. ICECIE, Aalborg, Denmark; 2019.
[30] Car M, Markovic L, Ivanovic A, Orsag M, Bogdan S. Autonomous wind-turbine blade inspection using lidar-equipped unmanned aerial vehicle. IEEE Access 2020;8:131380–7.
[31] Bortolotti P, Canet H, Bottasso CL, Loganathan J. Performance of non-intrusive uncertainty quantification in the aeroservoelastic simulation of wind turbines. Wind Energy Sci 2019;4:397–406.
[32] Papi F, Balduzzi F, Ferrara G, Bianchini A. Uncertainty quantification on the effects of rain-induced erosion on annual energy production and performance of a multi-mw wind turbine. Renew Energy 2021;165:701–15.
[33] Padulo M, Campobasso M, Guenov M. A novel uncertainty propagation method for robust aerodynamic design. AIAA J 2011;49:530–43.
[34] Campobasso M, Cavazzini A, Minisci E. Rapid estimate of wind turbine energy loss due to blade leading edge delamination using artificial neural networks. J Turbomach 2020;142. http://dx.doi.org/10.1115/1.4047186.
[35] Jonkman J, Butterfield S, Musial W, Scott G. Definition of a 5-MW reference wind turbine for offshore system development. Technical Report NREL/TP-500-38060, Golden, CO, USA: NREL; 2009.
[36] Han W, Kim J, Kim B. Effects of contamination and erosion at the leading edge of blade tip airfoils on the annual energy production of wind turbines. Renew Energy 2018;115:817–23.
[37] Castorrini A, Corsini A, Rispoli F, Venturini P, Takizawa K, Tezduyar TE. Computational analysis of wind-turbine blade rain erosion. Comput & Fluids 2016;141:175–83.
[38] Schramm M, Rahimi H, Stoevesandt B, Tamgager K. The influence of eroded blades on wind turbine performance using numerical simulations. Energies 2017;10:1–15.
[39] Sareen A, Sapre CA, Selig MS. Effects of leading edge erosion on wind turbine blade performance. Wind Energy 2014;17:1531–42.
[40] Bardal LM, Sætran LR. Influence of turbulence intensity on wind turbine power curves. Energy Procedia 2017;137:553–8.
[41] Berge E, Byrkjedal Ø, Ydersbond YW, Kindler D. Modelling of offshore wind resources. comparison of a mesoscale model and measurements from FINO 1 and north sea oil rigs. In: European wind energy conference. Marseille, France; 2009.
[42] Emeis S. Current issues in wind energy meteorology. Meteorol Appl 2014;21:803–19.
[43] RSE. Atlas eolico. 2022, atlanteeolico.rse-web.it. Milan, Italy. Accessed on 31 October 2022.
[44] Ren G, Liu J, Wan J, Li F, Guo Y, Yu D. The analysis of turbulence intensity based on wind speed data in onshore wind farms. Renew Energy 2018;123:756–66.
[45] Jonkman J, Sprague M. OpenFAST: An aeroelastic computer-aided engineering tool for horizontal axis wind turbines. Golden, Colorado: National Renewable Energy Laboratiry; 2022, www.nrel.gov/wind/nwtc/openfast.html. Accessed on 31 October 2022.
[46] Heyman G, Jonkman B, Murray R, Damiani R, Jonkman J. AERODYN: A time-domain wind and MHK turbine aerodynamics module. Golden, Colorado: National Renewable Energy Laboratiry; 2022, www.nrel.gov/wind/nwtc/aerodyn.html. Accessed on 31 October 2022.
[47] Jonkman B, Kilcher L. TurbSIm: A stochastic, full-field, turbulence simulator primarily for use with inflowwind/aerodyn-based simulation tools. Golden, Colorado: National Renewable Energy Laboratiry; 2022, https://www.nrel.gov/wind/nwtc/turbsim.html. Accessed on 31 October 2022.
[48] Ansys-Inc. Fluent theory guide, release 2019.r3. 2019, www.ansys.com/Products/Fluids/ANSYS-Fluent, Accessed on 31 October 2022.
[49] Menter F. Two-equation turbulence-models for engineering applications. AIAA J 1994;32:1598–605.
[50] Menter F, Langtry R, Likki S, Suzen Y, Huang P, Völker S. A correlation-based transition model using local variables – part I: Model formulation. J Turbomach 2006;128:413–22.
[51] Langtry R, Menter F, Likki S, Suzen Y, Huang P, Völker S. A correlation-based transition model using local variables – part II: Test cases and industrial applications. J Turbomach 2006;128:423–34.
[52] Langtry R, Menter F. Correlation-based transition modeling for unstructured parallelized computational fluid dynamics codes. AIAA J 2009;47:2894–906.
[53] Campobasso M, Castorrini A, Cappugi L, Bonfiglioli A. Experimentally validated three-dimensional computational aerodynamics of wind turbine blade sections featuring leading edge erosion cavities. Wind Energy 2022;25:168–89.
[54] Achenbach E, Heinecke E. On vortex shedding from smooth and rough cylinders in the range of Reynolds numbers 6×10^3 to 5×10^6. J Fluid Mech 1981;109:239–51.

[55] Ansys-Inc. Introduction to ansys ICEM CFD. 2022, www.ansys.com/training-center/course-catalog/fluids/introduction-to-ansys-icem-cfd, Accessed on 31 October 2022.
[56] High end computing. HEC, Lancaster University; 2022, www.lancaster.ac.uk/iss/info/ITh{and}outs/hec/HEC-flyer.pdf, Accessed on 22 April 2022.
[57] Timmer WA, Schaffarczyk AP. The effect of roughness at high reynolds numbers on the performance of aerofoil DU 97-w-300mod. Wind Energy 2004;7:295–307.
[58] Fuglsang P, Bak C. Development of the Risø wind turbine airfoils. Wind Energy 2004;7:145–62.
[59] Campobasso M, Minisci E, Caboni M. Aerodynamic design optimization of wind turbine rotors under geometric uncertainty. Wind Energy 2014;19:51–66.
[60] Hahn GJ, Shapiro SS. Statistical models in engineering. 2nd ed.. Hoboken, NJ: John Wiley and Sons; 1994.
[61] Langreder W, Kaiser K, Hohlen H, Højstrup J. Turbulence correction for power curves. In: European wind energy conference. London, UK; 2004.